ACS Catalysis

Research Article

pubs.acs.org/acscatalysis

Determination of Iron Active Sites in Pyrolyzed Iron-Based Catalysts for the Oxygen Reduction Reaction

Wenmu Li, Jason Wu, Drew C. Higgins, Ja-Yeon Choi, and Zhongwei Chen*

[†]Department of Chemical Engineering, Waterloo Institute for Nanotechnology, Waterloo Institute for Sustainable Energy, University of Waterloo, 200 University Avenue West, Waterloo, Ontario, Canada N2l 3G1

Supporting Information

ABSTRACT: Fe-based oxygen reduction reaction (ORR) catalyst materials are considered promising nonprecious alternatives to traditional platinum-based catalysts. These catalyst materials are generally produced by high-temperature pyrolysis treatments of readily available carbon, nitrogen, and iron sources. Adequate control of the structure and active site formation during pyrolysis methods is nearly impossible. Thus, the chemical nature, structure, and ORR mechanism of catalytically active sites in these materials is a subject of significant debate. We have proposed a method, utilizing CN^- ions as ORR inhibitors on Fe-based catalysts, to provide insight into the exact nature and chemistry of the catalytically active sites. Moreover, we propose two possible catalytically active site formation mechanisms occurring during high-temperature pyrolysis treatments, dependent on the specific type of precursor and synthesis methods utilized. We have further provided direct evidence of our proposed active site formations using ToF-SIMS negative and positive ion imaging. This knowledge will be beneficial to future work directed at the development of Fe-based catalysts with improved ORR activity and operational stabilities for fuel cell and battery applications.

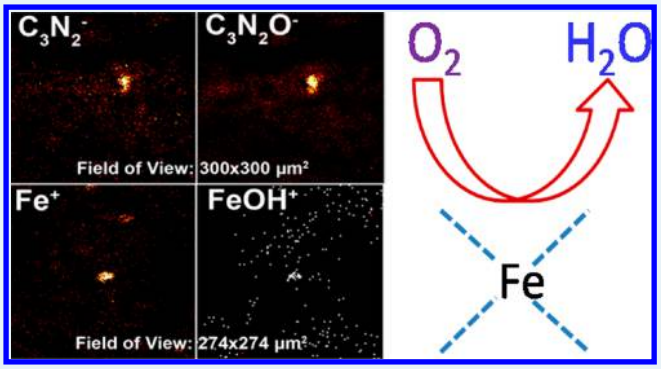

KEYWORDS: *fuel cell, Fe-based catalysts, chemical model, active site*

INTRODUCTION

Fe−N_x/C electrocatalysts (Fe-based catalysts) for the oxygen reduction reaction (ORR) are widely studied due to their promising performance in fuel cell and battery applications.[1,2] Fe-based catalysts can be obtained through high-temperature pyrolysis of either iron N_4 chelate complexes,[3−7] or simple precursors consisting of an iron salt, a nitrogen source (aromatic[8−10] and aliphatic ligands[11−15] or other nitrogen-rich small molecules[16−21]) and a carbon support. Through these methods, highly active or stable iron-based catalysts have successfully been obtained.[22,23] This creates an illusion that regardless of which nitrogen-containing precursors, carbon source, and synthesis techniques are used for catalyst synthesis, the resulting catalytically active sites should be similar. However, the ORR mechanistic pathway on iron-based catalysts is far more complicated than that of platinum catalysts. It is governed by the distinct electronic and geometric properties of the metal ion and by the surrounding environments, where even small changes will result in different oxygen activation mechanistic pathways. The uncertainty and difficulty in elucidating and controlling the exact nature of these catalytically active sites makes further development and optimization of these catalysts a significant challenge. Therefore, to date, trial-and-error or combinatorial approaches have been used in the development of heat-treated Fe-based catalysts. Developing a method to identify the chemical properties of ORR active sites is of significant importance in the research and development of Fe-based catalysts for PEMFC applications.

The current proposed active sites are mainly speculated by data obtained from X-ray photoelectron spectroscopy (XPS),[7,24,25] time-of-flight secondary ion mass spectroscopy (ToF-SIMS),[16] X-ray absorption fine structure,[6,16] and mossbauer spectroscopy[5,7] and are based upon the possible configurations of Fe and N, their atomic ratios, or theoretical calculations.[26] On the basis of these techniques, edge plane FeN_2/C and FeN_4/C[16] species as well as basal plane macrocyclic FeN_4/C species[3,7] have been proposed as the active site structures, accordingly. However, although these methods provide hypotheses of the active site structures, the key properties influencing catalyst activity and stability, such as coordination chemistry and geometric structures of the active sites, has not been unveiled. The debatable nature of the active site structures has even led to the hypothesis that the iron itself is not a part of the active site, that it merely facilitates the formation of catalytically active N/C structures.[27,28]

The general approach in determining whether iron is the active center has traditionally involved the use of small molecules to interrupt the Fe−O_2 interactions by the formation of highly

Received: March 26, 2012
Revised: October 22, 2012
Published: October 24, 2012

   dx.doi.org/10.1021/cs300579b | ACS Catal. 2012, 2, 2761−2768

stable iron−ligand coordination intermediate compounds. Strong ligands, such as CO and CN^-, have been proposed as adequate inhibitors for this purpose.[29] However, recently it has been demonstrated that CO molecules are not suitable inhibitors for blocking of ORR active sites.[30] This is because the binding affinity of small molecules to iron ion centers depends mainly on the chemical composition of the active sites (i.e., ligands, geometric structures, and iron valence), and CO molecules have been found to be ineffective in blockage of several Fe species because of the low CO−Fe(II) affinity. Thus, CN^- ions, the strongest single ligand, have been chosen as the optimal small molecular inhibitor to identify whether Fe centers comprise the ORR active sites in these catalytic materials.[31−33] However, we believe that the capability of these methods has not fully been exploited, which is the subject of the present paper. The information provided in this study permits the effective screening of potential catalysts and will provide a basis for optimization of synthesis methods.

In the present paper, CN^- ions were applied as blocking molecules to inhibit different Fe-based catalysts toward the ORR. Specifically, the Fe-based catalysts utilized include (i) the model compound ferrous 2,9,16,23-tetra(2′,6′-diphenylphenthio ether)phthalocyanine (Fe-SPc), (ii) the famous ammonia-treated iron-based (Fe-NH_3/C), (iii) pyrolyzed cyanamide−iron salt (Fe-Cy/C), (iv) pyrolyzed aromatic 2,3,7,8-tetra-(pyridin-2-yl)pyrazino[2,3-*g*]quinoxaline iron complexes (Fe-TPPQ/C), and (v) pyrolyzed simple commercially available iron phthalocyanine-based catalysts (Fe-Pc/C). These materials were all prepared, and their ORR chemistries toward the CN^- ion were analyzed accordingly. Our experiments reveal that the resistance of Fe-based catalysts to CN^- inhibition was strongly affected by the specific choice of precursor materials and preparation procedures.

RESULTS AND DISCUSSION

The polarization curves for Fe-SPc/C, Fe-Pc/C, Fe-TPPQ/C, Fe-NH_3/C, and Fe-Cy/C in 0.1 M NaOH at a rotation speed of 400 rpm are shown in Figures 1 and 2. The insets in Figures 1 and 2 also show the associated ring currents for each of the catalysts. All catalysts display recognizable and well limiting currents. Upon introducing 10 mM KCN into the electrolyte, noticeable changes in the ORR behavior of the Fe-SPc/C, Fe-Pc/C, Fe-NH_3/C, and Fe-Cy/C catalysts is observed. In these catalysts, significant loss of limiting current is observed. The Fe-TPPQ/C catalyst exhibited a very small loss in its limiting current when exposed to CN^- ions. After thoroughly washing the catalysts to remove bound CN^- ions, the Fe-SPc/C, Fe-Pc/C, and Fe-TPPQ/C catalysts recover most of its lost current, showing the same ORR activity as before CN^- poisoning. Neither the Fe-NH_3/C nor Fe-Cy/C catalysts showed complete recovery of its original activity after washing. The Fe-NH_3/C catalyst showed no recovery of activity, whereas the Fe-Cy/C catalyst only showed some recovery of its original activity.

The ring currents follow a similar trend as with the disk currents. The Fe-SPc/C and Fe-Pc/C catalysts exhibit the same behavior in generation of ring current: both catalysts show increased generation of ring current after CN^- poisoning. Once the CN^- ions are removed, the ring current drops back to the same level as prior to poisoning the catalysts. The Fe-TPPQ/C, Fe-NH_3/C, and Fe-Cy/C catalysts displayed higher ring currents after electrode washing, suggesting that the introduction of CN^- ions may result in the formation of compounds that may assist in the reduction of hydrogen peroxide. The CN^- poisoning

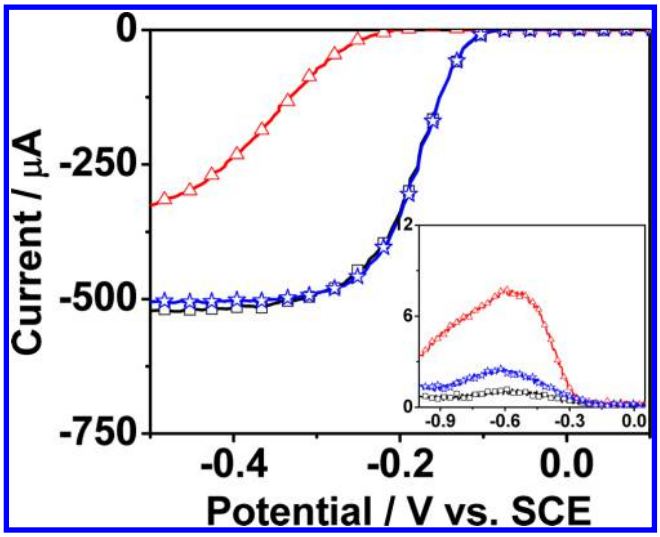

Figure 1. Polarization curves for the ORR (□) in 0.1 M NaOH without CN^-; (△) with 10 mM CN^-; and (☆) after CN^- poisoning tests, electrode washing, and immersion in fresh 0.1 M NaOH for Fe-SPc/C. Curves were obtained at a sweep rate of 10 mV s^{-1} from −1.0 to 0.2 V vs SCE, with an electrode rotation speed of 400 rpm. Inset: ring currents obtained during ORR testing.

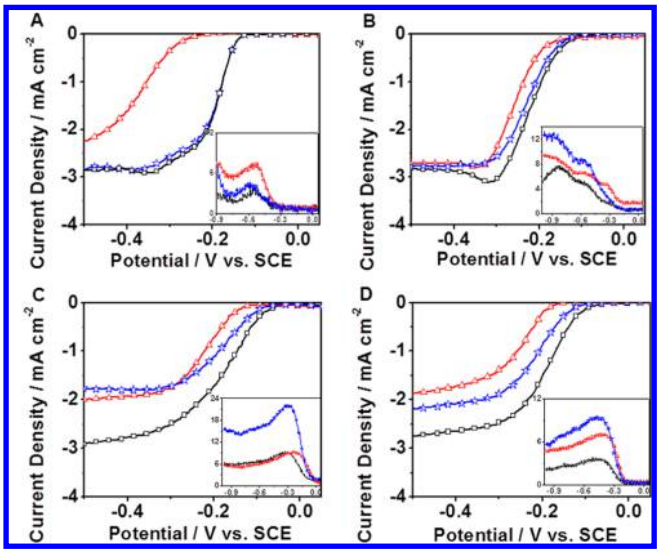

Figure 2. Polarization curves for the ORR (□) in 0.1 M NaOH without CN^-; (△) with 10 mM CN^-; and (☆) after CN^- poisoning tests, electrode washing and immersion in fresh 0.1 M NaOH for heat treated (A) Fe-Pc/C-800,)B) Fe-TPPQ/C-900, (C) Fe-NH_3/C-900, and (D) Fe-Cy/C-900. Curves were obtained at a sweep rate of 10 mV s^{-1} from −1.0 to 0.2 V vs SCE, with an electrode rotation speed of 400 rpm. Inset: ring currents obtained during ORR testing.

behavior of the catalysts can be explained by examining and discussing the proposed active site structures present in nonprecious catalysts.

The proposed structures of high-temperature-treated Fe-based catalysts are depicted in Scheme 1. These active sites include 1,10-phenanthroline (phen)-like iron complexes (**A** and **C**),[16,19,20] single pyridine-like iron complexes (**B** and **E**), and macrocyclic-like iron complexes (**D** and **F**).[3,7] The performance of synthesized Fe-based catalysts has been directly related to increasing amounts or combinations of these active sites in the catalyst materials. Furthermore, the difference in response to CN^- poisoning between the catalysts investigated can be

dx.doi.org/10.1021/cs300579b | *ACS Catal.* 2012, 2, 2761−2768

Scheme 1. Possible Iron Active Site Structures on Nanocrystal Graphite: (a) Top and (b) Side View

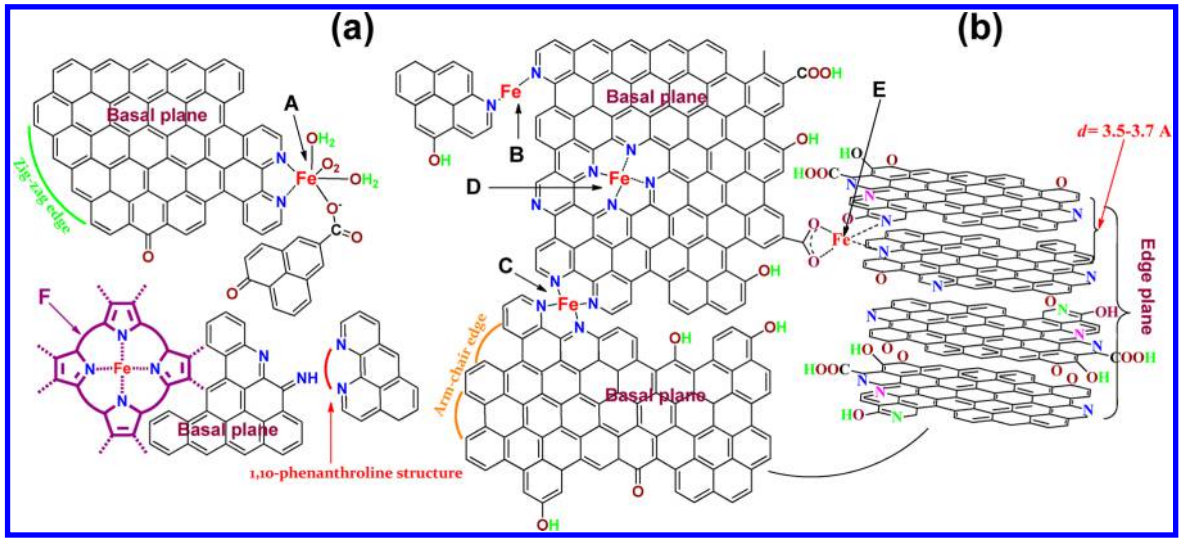

attributed to the types or composition of active sites present within the catalysts after the high-temperature treatment.

It is highly likely that the choice of catalyst precursors and preparation methods greatly influences the types of active sites available after synthesis. Both Fe-Pc and Fe-TPPQ/C are synthesized employing aromatic nitrogen precursors and, especially in the case of Fe-Pc/C, display responses to CN^- poisoning that are similar to that of the macrocyclic complex, Fe-SPc/C. The nearly identical CN^- poisoning behavior in disk and ring current between Fe-Pc/C and Fe-SPc/C suggests that the Fe-Pc/C catalyst contains a majority of active sites that are very similar to that of macrocyclic complexes. Although not as pronounced, Fe-TPPQ/C also displays similar current loss and recovery behavior when introduced to CN^- ions. The remaining two catalysts are synthesized utilizing small nonaromatic ligands: ammonia and cyanamide for Fe-NH_3 and Fe-Cy, respectively. Fe-NH_3/C and Fe-Cy/C show similar incomplete recovery of activity after CN^- poisoning and electrode washing as well as high ring currents after CN^- removal. This result suggests that Fe-NH_3/C and Fe-Cy/C catalysts consist of a majority of active sites that differ from macrocyclic complexes and are unstable when exposed to CN^- ions.

A short discussion regarding the nature of the reactions occurring between these different iron complexes and other strong ligands or proton species is necessary because these reactions can provide us with a foundation to isolate different active sites on the basis of simple chemistry. The phen-like complexes are well established active site structures, and the simple phen ligand itself is considered the strongest bidental ligand available. Thus, if we can successfully replace these iron-anchored phen ligands with other small molecules, it will be possible to apply this replacement reaction to any other type of readily available bidental ligand. The CN^- ions could readily react with the most stable $[Fe(phen)_3]^{2+}$ to form different mixed ligand iron complexes, such as dicyano-bis-phen ferrate (2), tetracyano-monophen ferrate (3), and $[Fe(CN)_6]^{4-}$ (4) (Scheme 2), although the reactions themselves are reversible.[34,35] Therefore, in CN^- ion poisoning tests, the active site A will react with excess CN^- ions to form stable mixed ligand-iron complexes (3) or even the $[Fe(CN)_6]^{4-}$ structure. The ORR will not be successfully catalyzed by these complexes because of the fact that the ORR itself is an inner-sphere electron reaction, and

Scheme 2. The Chemical Reactions between $Fe(phen)_3$ and Cyano Groups

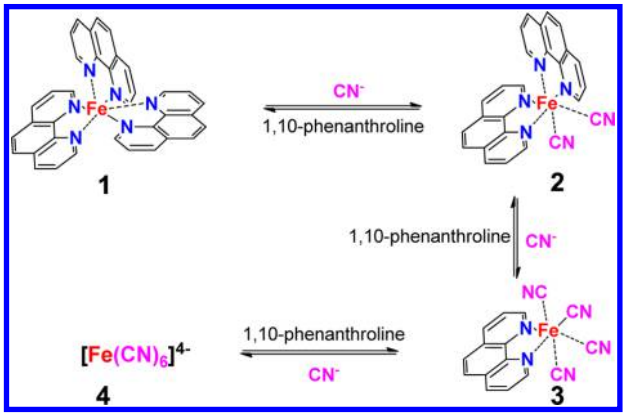

both ligand CN^- and phen binding are too strong to be replaced by O_2 molecules. Thus, the ORR currents contributed by these active sites are not recoverable after CN^- ion poisoning has taken place. This is also applicable to other less-strong ligand–iron complexes, **B** and **E**.

Conversely, this CN^- ion poisoning chemistry may not be applicable in the case of iron macrocycle complexes, such as semimacrocyclic-like (**C**) and macrocyclic (**D** and **F**) active site structures. Although the latter is considered a phen-like structure, its in-plane structure renders CN^- replacement of the large graphitic ligands unfavorable because of the steric hindrance of this complex. Extensive studies have been focused on the interactions between CN^- ions and heme proteins,[29,36] providing us with adequate models to decipher the exact mechanism and active site structures of the ORR on similar active site structures. Although the results are extensive and complicated, widespread consensus on the extremely poor stability of heme–Fe(II)–CN complexes has consistently been reported. Therefore, in most heme proteins, ferrous cyanide complexes are considered as a transient intermediate species following the reduction of the ferric cyanide adduct. In fact, the metastable ferrous porphyrin CN^- was not successfully synthesized until 2008 because of the poor stability of these materials.[37] In comparison, their counterpart, heme–Fe(III)–CN is a highly stable complex. The equilibrium constant for

dx.doi.org/10.1021/cs300579b | ACS Catal. 2012, 2, 2761–2768

Scheme 3. Possible Mechanism of CN^- Blocking on FePc Catalysts for ORR

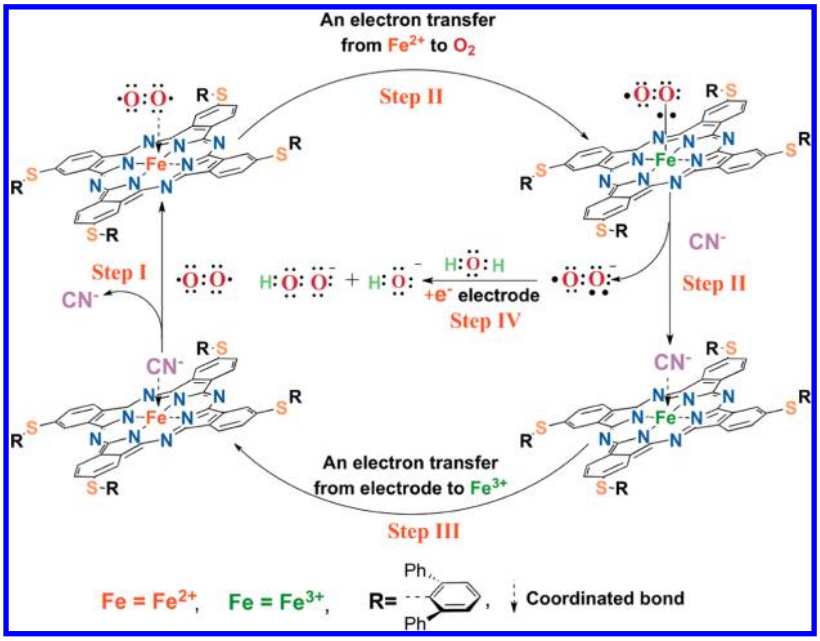

cyanide binding to most iron(III) hemeproteins is often $\geq 10^5$ M^{-1}, compared with no more than 10^2 M^{-1} for iron(II) species.[36] This low equilibrium constant of heme−Fe(II)−CN indicates that cyano ions may readily be replaceable by oxygen molecules.

We believe that this specific chemistry involving cyano binding to heme proteins may be applicable to other iron macrocycle complexes. To verify our assumption, we have previously utilized Ketjen-300 carbon black-supported Fe-SPc (Fe-SPc/C) as a model compound to investigate the CN^- poisoning effects, and a correlative mechanism was proposed.[32] The proposed CN^- poisoning mechanism of Fe-SPc can be found illustrated in scheme 3. With respect to this mechanism, one important issue was still prominent. The complete recovery of ORR activity following CN^- poisoning was expected since the demetalation of Fe-SPc and stable SPc-Fe(II)−CN may not occur during CN^- poisoning experiments. In Figure 1, it can be seen that the recovery of the major ORR current and a decrease in the ring current after poisoning tests served to confirm our assumption that the CN^- on the unstable SPc-Fe(II)−CN complexes are replaceable by oxygen molecules and demetalation of the iron complex did not occur. Herein, we propose that these conclusions may be applicable toward other iron macrocycle (active site **D** and **F**) and semimacrocycle-like complexes (in-plane **C**). We believe that in-plane **C** may behave like macrocyclic iron complexes because the geometric structure of site **C** is sterically restricted since this tiny site resides on the edge plane of the two big, insoluble nanocrystal graphites. This molecular configuration is very difficult to produce and isolate because it requires encapsulation by these bulky graphitic three-dimensional arrays, forming a confined atomic configuration similar to iron macrocyclic structures.

In an attempt to produce **D** and in-plane **C** sites, two Fe-based catalysts—Ketjen 600 carbon black-supported aromatic Fe-TPPQ/C- and Fe-Pc/C-based catalysts treated at 900 °C for 1 h (Fe-TPPQ/C-900) and 800 °C for 20 min (Fe-Pc/C-800), respectively—were prepared. These compounds were selected because they contain favorable initial structures that after pyrolysis have the best chances at retaining a similar atomic arrangement to form active site structures **C** and **D**.[7] Linear sweep curves for these materials in 0.1 M NaOH are provided in Figure 2, displaying initial ORR activity, activity in the presence of CN^- (10 mM), and activity after electrode rinsing with DI water and immersion into a fresh electrolyte solution (Figure 2A and B). Our results demonstrated that both of these catalysts displayed similar CN^- poisoning patterns with that of Fe-SPc/C, where the majority of the limiting currents following CN^- poisoning are recovered after electrode washing. Thus, this indicates that our speculation appears concise in that sites **C** and **D** display chemistries similar to that of phthalocyanine complexes, which have previously been demonstrated to be similar to that of porphyrin and heme materials. We conclude that in Fe-Pc/C-800 and Fe-TPPQ/C-900, there exists a very high ratio of relatively stable macrocycle-like active sites (**C** and **D**) to the unstable sites (**A**, **B** and **E**) in these catalyst materials. This analysis is consistent with previous reports indicating superior stability of FeN_4/C species in comparison with FeN_2/C.[16] We cannot, however, exclude the existence of these unstable active sites because any combination of structures may form in the process of high-temperature pyrolysis. This can offer a reasonable explanation for the minimal loss of performance observed after CN^- poisoning and electrode washing.

Although Fe-TPPQ/C displayed a CN^- poisoning profile similar to that of Fe-Pc/C and Fe-SPc/C, Fe-TPPQ/C also exhibits a pronounced resistance to CN^- poisoning, only experiencing limited current loss compared with that of Fe-Pc/C or Fe-SPc/C. The uncanny resistance toward CN^- poisoning could be attributed to the preparation method for the catalysts and the nitrogen precursors TPPQ and Fe-Pc. The Fe-Pc is molecule that is 1.6 nm in diameter with a propensity to aggregate,[38,39] whereas TPPQ is a much smaller ligand designed to be highly soluble in polar solvents. This allows the TPPQ ligand to better penetrate and impregnate the micropores of the carbon support prior to high-temperature pyrolysis, resulting in active site formations within the micropores of the carbon support. In contrast, the micropores of the carbon support are not fully accessible to the majority of the Fe-Pc macrocycles, and thus, active site formation is largely limited to the surface of the carbon support. During CN^- poisoning, CN^- ions cannot readily

dx.doi.org/10.1021/cs300579b | ACS Catal. 2012, 2, 2761−2768

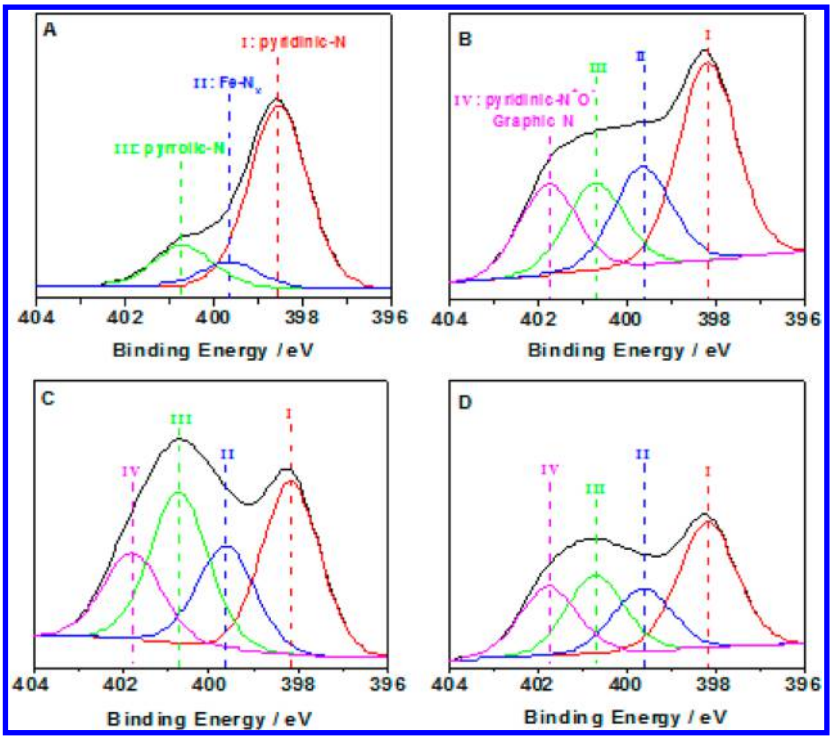

Figure 3. N 1s narrow scan of spectra of heat-treated (A) Fe-Pc/C-800, (B) Fe-TPPQ/C-900, (C) Fe-NH_3/C-900, and (D) Fe-Cy/C-900.

block certain active sites located within the micropores because these active sites are inaccessible to the ions. The highly hydrophobic nature of the micropores prevents water from carrying CN^- ions to the iron active sites; however, water is still able to penetrate the micropores because of liquid−vapor oscillations,[40] allowing water to continue to play its role in the reaction.[41]

The specific nature and surface density of different active sites present in the final catalysts will strongly depend on the choice of precursor materials and the exact synthesis procedures utilized. We propose that active site formation can occur by two mechanisms during high-temperature pyrolysis: When utilizing aromatic iron complex ligands in inert atmospheres, catalytically active sites will be formed in the layers of material deposition and will build up on the surface of the carbon support. With active site formation of this nature, the accumulated surface layers will not be highly porous, such that only the surface layer containing the most outer active sites is accessible. This will not only result in the majority of active sites being inaccessible, entrapped in the subsurface layers, but will also cause blockage of small pores and channels present in the carbon support, leading to inhibited reactant and product mass transfer to and from the catalytically active sites.

The second active site formation mechanism involves etching of the carbon support material with oxidative compounds, resulting in the simultaneous production of active sites and well connected channels. Small nonaromatic ligands, such as NH_3, and aliphatic diamines can result in active site formation of this nature. The alteration of the carbon support materials and active site formation mechanisms are extremely different when using aromatic ligand precursors compared with utilization of small etching molecules, such as NH_3, and ethylenediamine. In the latter case, because of the thermal instability and high reactivity with carbon supports at high temperatures, these small molecules target amorphous carbon species for surface etching.[20] Therefore, it is likely that the ratios of relatively unstable (**A**, **B**, and **E**) to stable active sites (in-plane **C** and **D**) should be much higher for catalysts synthesized using small etching molecules than for that of catalysts obtained from aromatic ligand precursors. The CN^- poisoning behaviors (Figure 2C and D) of Fe-NH_3/C and Fe-Cy/C, prepared by utilizing ammonia and cyanamide as nitrogen precursors, support this hypothesis. These two catalyst materials were exposed to CN^- ion poisoning tests to gain insight regarding the nature of the active sites formed. Both Fe-NH_3/C and Fe-Cy/C catalysts displayed a loss of current after CN^- ion poisoning tests, even after thorough electrode washing (Figure 2C and D, respectively). This loss of activity was especially prominent in the case of the Fe-NH_3 catalyst, in which the limiting current after electrode washing was even lower than the limiting current obtained in the presence of 10 mM KCN. This significant loss of current observed following CN^- ion poisoning is attributed to the high density of relatively unstable active sites (**A**, **B** and **E**) in a catalyst prepared by ammonia treatment methods, which is consistent with our proposed model. Fe ions present in these unstable active sites may also have reacted with CN^- ions to form $[Fe(CN)_6]^{4-}$ complexes, which is considered a very good hydrogen peroxide reduction reaction (HPRR) catalyst.[42] Low ring currents during CN^- ions poisoning tests support this claim, an indication that formed $[Fe(CN)_6]^{4-}$ species were adsorbed onto the surface of the carbon support and would further reduce any H_2O_2 byproduct species formed. After electrode washing, the $[Fe(CN)_6]^{4-}$ ions are effectively removed, as indicated by significantly increased ring currents and reduced ORR diffusion-limited currents in the Fe-TPPQ/C, Fe-NH_3/C, and Fe-Cy/C catalysts (Figure 2B, C, and D). This provides a reasonable explanation as to why using small molecules as nitrogen sources to make stable Fe-based catalysts can be quite difficult, despite numerous reports indicating that ammonia treatment methods are the optimal way of producing high-activity Fe-based catalyst materials. Indeed, the best Fe-based catalysts to date were obtained through the pyrolysis of aromatic ligands with $Fe(OAc)_2$ in an inert atmosphere first.[22]

dx.doi.org/10.1021/cs300579b | *ACS Catal.* 2012, 2, 2761−2768

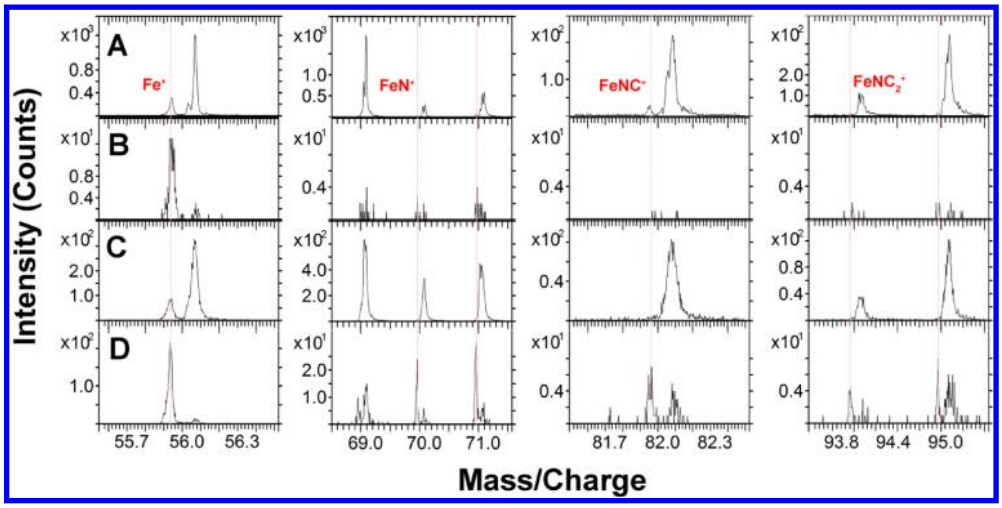

Figure 4. ToF SIMS positive ion spectra of (A) Fe-Pc/C-800, (B) Fe-TPPQ/C-900, (C) Fe-NH_3/C-900, and (D) Fe-Cy/C-900.

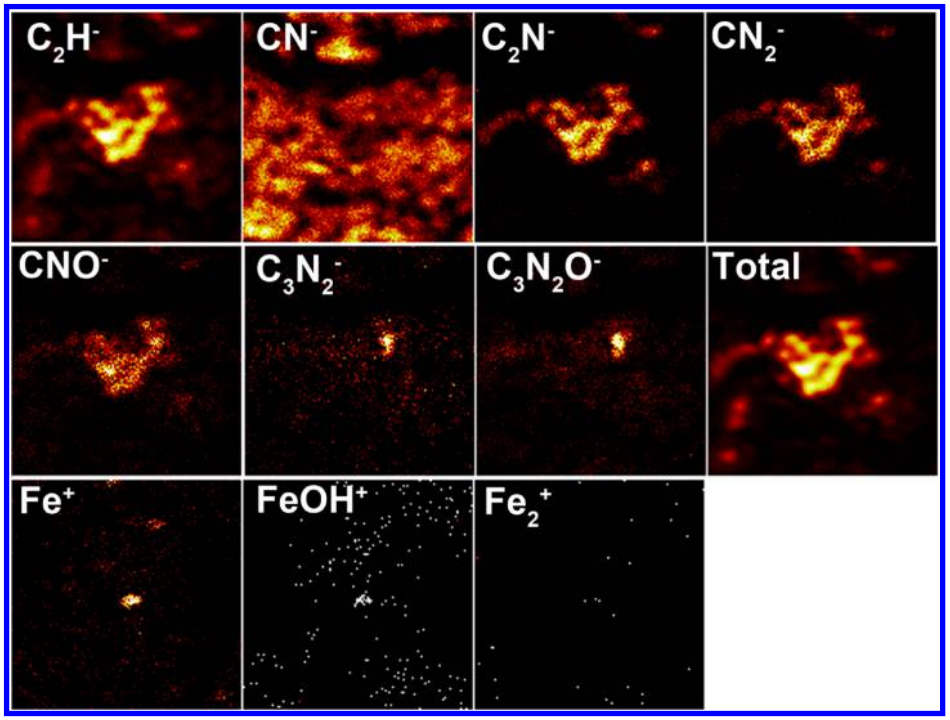

Figure 5. ToF SIMS $C_xN_y^-$ negative ions (field of view: 299.8 × 299.8 μm) and Fe^+ positive ion (field of view: 274.4 × 274.4 μm) images of Fe-TPPQ/C-900 catalyst, showing spatial origin of ions.

This could potentially result in the formation of highly stable catalytically active sites; however, the blocking of these active sites serves as an inhibitor to high activity. Thus, after further exposing these catalyst materials to high-temperature treatments in ammonia, pore etching occurs, allowing significantly higher porosities and increased access to the catalytically active sites.

To verify the composition of the investigated catalysts, the high-resolution N(1s) XPS spectra of the heat-treated catalysts was determined (Figure 3). Peak I (398.2 eV) and peak III (400.7 eV) can be assigned to pyridinic (397−399.5 eV) and pyrrolic (400.2−400.9 eV) nitrogen groups, whereas peak II (399.6 eV) can be regarded as N-bonded to a metal center in an Fe−N_x configuration (399−400.5 eV).[3,25] The associated iron scans included in the Supporting Information (Figure S4) for Fe-Pc/C, Fe-TPPQ/C, and Fe-Cy/C catalysts shows iron exists in mostly Fe(II) or Fe(III) states, with peaks located at 707.4 and 710.5 eV, respectively.[3,8]

The Fe2p spectra of all three catalysts show very similar peak intensities and locations, suggesting that the electronic state of iron within all three catalysts is likely the same. Because of extremely low surface iron content in the Fe-NH_3/C catalyst, an Fe spectrum could not be resolved within the same collection time. In the case of heat-treated Fe-Pc/C, the N(1s) spectrum displays a shift in the binding energy to 398.6 eV. This strong peak is consistent with previous reports on Fe-Pc/C,[24] attributed to the similar binding energies of all nitrogen species in FePc complexes. Moreover, it was reported that above 700 °C, the decomposition of FePc will initiate, forming nitrogen species responsible for the emergence of peaks II and III.[24] The small magnitude of this shoulder observed at higher binding energies indicates that a significant portion of the FePc core structures still

dx.doi.org/10.1021/cs300579b | ACS Catal. 2012, 2, 2761−2768

remain intact following our pyrolysis procedure. Supporting this, the response to CN^- ion blocking of pyrolyzed Fe-Pc/C was almost identical to that of the nonpyrolyzed model catalyst Fe-SPc/C, indicating similar active site structures on the two materials.

Now, to correlate the observed N(1s) signals with the electrochemical behavior demonstrated by the catalysts presented in this work, the following speculations can be made: Increases in the peak II intensity are attributed to higher Fe center coordination. This is due to the fact that a higher number of the nitrogen atoms scanned through high-resolution XPS are coordinated to Fe metal centers (i.e., higher x values in Fe−N_x). This indicates that for Fe-TPPQ/C (Figure 3B), the presence of chemically stable Fe−N_4 species is more prominent. Conversely, Fe-NH_3/C and Fe-Cy/C have reduced peak II intensities (Figure 3C and D, respectively). This can be attributed to the increased density of active sites **A**, **B**, and **E** with low iron center coordination and chemical instability. Thus, it is possible that the increased intensity of peak II observed by XPS can be attributed to a higher nitrogen coordination number of Fe centers, in direct agreement with the CN^- poisoning experiment results.

By utilizing ToF-SIMS, several researchers have proposed active site structures based on the ion emissions detected by mass spectroscopic techniques.[16,19,43] Generally, the ion fragments of interest consist of Fe (or Co), coordinated with N and C, labeled for brevity as $FeN_xC_y^+$. When analyzing ToF-SIMS signals, there is often convolution between fragments containing Fe and fragments free of Fe. For example, with limited signal resolution, $C_2H_4N_2^+$ ions with a molecular weight of ∼56.04 can easily be convoluted and misinterpreted as Fe^+ ion signals with a molecular weight of ∼55.94. Thus, by exercising caution when interpreting ToF-SIMS results, it is possible to adequately identify the Fe-containing surface moieties present in the electrocatalyst samples. Utilizing this knowledge, ToF-SIMS data was obtained for each catalyst sample and is displayed in Figure 4. From the obtained positive mode spectra, $FeNC^+$ and $FeNC_2^+$ ions were the only Fe/N-containing species that could be positively confirmed. Acquired signals at molecular weights beyond 93.94 were observed, but could not be distinctly attributed to high-molecular-weight $FeN_xC_y^+$ as a result of convolution with a wide variety of ion configurations. However, on the basis of ToF-SIMS negative and positive ion imaging of the Fe-TPPQ/C-900 in Figure 5, there is direct evidence that the detected Fe^+, $C_3N_2^-$, and $C_3N_2O^-$ fragments originate from the same spatial location. From these results, we can infer that there is a high possibility that the fragments are of the FeN_4C_x type of active sites (**C**, **D**, and **F**). The combined ToF-SIMS and CN blocking results provides indication that Fe ion-based centers are most likely the primary site of ORR on the surface of these investigated materials.

CONCLUSION

In conclusion, an improved method of utilizing CN^- ions as inhibitors on Fe-based ORR catalyst materials has been developed in order to gain valuable insight regarding the exact nature and chemistry of catalytically active sites. This method was developed on the basis of simple chemistry and well documented Fe−CN^- interaction mechanisms, along with experimental results obtained using several different Fe-based electrocatalyst materials. We propose two active site formation mechanisms that occur during high-temperature pyrolysis, dependent on the type of precursor materials utilized, which significantly influence the activity and stability of these materials. We further confirm our hypothesis with ToF-SIMS negative and positive ion imaging to provide information regarding the composition and the possible chemical structure of active sites. These methods and mechanisms will provide valuable insight toward the development of Fe-based catalysts with improved ORR activity and stability.

EXPERIMENT AND METHODS

Ferrous 2,9,16,23-tetranitro phthalocyanine (Fe-SPc)[32] and 2,3,7,8-tetra(pyridin-2-yl)pyrazino[2,3-g]quinoxaline(TPPQ)[44] were prepared in a method discussed in our previous papers. High-temperature-treated Fe-based catalysts supported on Ketjen-600 (Fe-TPPQ/C-900, [30] Fe-Pc/C-800,[33] Fe-NH_3/C,[16] and Fe-Cy/C[15]) were prepared following previously reported procedures from other laboratories. Fe-SPc catalysts were synthesized beginning with 1.73g of 4-nitrophthalonitrile and 0.43g of Fe(II) acetate in 100 mL of quinoline. The mixture was stirred and heated to 210 °C for 24 h under a N_2-saturated atmosphere. The resulting crude product was filtered and purified. A 0.50 g portion of the purified product was added to a mixture of 2,6-diphenylthiophenol (0.72g) and Cs_2CO_3 (1g) in 10 mL of NMP and 10 mL of toluene. The mixture was stirred and heated to 180 °C for 12 h under N_2 protection. The resulting product was collected, filtered, washed with methanol, and purified. Fe-TPPQ catalysts were prepared by adding 7 mg of Fe(II) acetate into a solution of 10 mg of the TPPQ ligand in 20 mL of DMF. The mixture was stirred and heated to 150 °C under protection of N_2 gas for 1 h before adding 100 mg of carbon black (Ketjen Black EC600). After mixing for an additional hour, the catalyst was filtered and washed before entering high-temperature pyrolysis at 900 °C for 1h.

Fe-Pc/C-800 catalysts were prepared starting with a suspension of 20 mg of Fe(II) phthalocyanine in 10 mL of concentrated sulfuric acid. A 0.50 g portion of carbon black (Ketjen Black EC600) was added, and the suspension was sonicated for 2 h before being filtered, rinsed, and dried overnight. Pyrolysis of the dried product was done at 800 °C in an inert atmosphere for 20 min.

Fe-NH_3/C catalysts were prepared by prepyrolysis of the commercial dye, PTCDA, at 900 °C for 1 h under a mixture of NH_3, H_2, and Ar gas. Sufficient iron(II) acetate is adsorbed onto the prepyrolyzed PTCDA to achieve an iron content of 0.2 wt %, and after drying, the mixture is pyrolyzed at 900 °C under flow of NH_3, H_2, and Ar gas. Fe-Cy/C catalysts were prepared by mixing 0.5 g of FeSO4 and 0.5 g of carbon black (Ketjen Black EC600) in 125 mL of ethanol. The dispersion was heated to evaporate the ethano,l and the resulting iron-loaded carbon black was pryolyzed at 1000 °C for 1 h. The chemical structures of the TPPQ ligand, Fe-SPc, and FePc are shown in Figure S3 in the Supporting Information. Catalyst inks were created (4 mg catalyst/2 mL ethanol), and a 20 μL aliquot was deposited on a glassy carbon electrode and allowed to dry.

All electrochemical tests were carried out in a standard three-electrode configuration using a potentiostat (CH instruments) and 0.1 M NaOH electrolyte solution. A standard calomel reference electrode (SCE) was utilized along with a platinum wire counter electrode. The CN poisoning test was investigated by sweeping the potential from 0.2 to −1.0 V vs SCE. Scanning was carried out at 10 mV s^{-1} with a rotation speed of 400 rpm.

XPS analysis of the samples was performed using a Thermo Scientific K-Alpha XPS spectrometer. The samples were run at a takeoff angle of 90° using an Al Kα X-ray source with a spot area

dx.doi.org/10.1021/cs300579b | ACS Catal. 2012, 2, 2761−2768

of 400 μm. The samples were analyzed using an ION-ToF (Gmbh) ToF-SIMS IV equipped with a Bi liquid metal ion source. Powders were pressed onto a carbon tape. A 25 keV Bi^{3+} cluster primary ion beam pulsed at 10 kHz with a pulse width of 22 ns, and a target current of ~1 pA was used to bombard the sample surface to generate secondary ions. The secondary ions were extracted with an electric field of 2 keV from the sample surface, mass-separated, and detected via a reflectron-type time-of-flight analyzer, allowing parallel detection of ion fragments having a mass/charge ratio up to 900 within each cycle (100 μs). The postacceleration electric field was 10 keV. A pulsed, low-energy electron flood was used to neutralize sample charging. The spectra were calibrated with H and C peaks. For negative (positive) secondary ion mass spectra obtained on the substrate (carbon tape), the mass resolution for C^- (CH_3^+) and C_2H^- ($C_2H_3^+$) was 2600 (4000) and 4500 (5600), respectively.

■ ASSOCIATED CONTENT

Supporting Information

Scheme S1, Figures S1−S4, and Table S1. This information is available free of charge via the Internet at http://pubs.acs.org/.

■ AUTHOR INFORMATION

Corresponding Author

*E-mail: zhwchen@uwaterloo.ca.

Notes

The authors declare no competing financial interest.

■ ACKNOWLEDGMENTS

This work was financially supported by the Natural Sciences and Engineering Research Council of Canada (NSERC) and the University of Waterloo

■ REFERENCES

(1) Chen, Z.; Higgins, D.; Yu, A.; Zhang, L.; Zhang, J. *Energy Environ. Sci.* **2011**, *4*, 3167−3192.
(2) Jaouen, F.; Proietti, E.; Lefevre, M.; Chenitz, R.; Dodelet, J. P.; Wu, G.; Chung, H. T.; Johnston, C. M.; Zelenay, P. *Energy Environ. Sci.* **2011**, *4*, 114−130.
(3) Arechederra, R. L.; Artyushkova, K.; Atanassov, P.; Minteer, S. D. *ACS Appl. Mater. Interfaces* **2010**, *2*, 3295−3302.
(4) Koslowski, U. I.; Abs-Wurmbach, I.; Fiechter, S.; Bogdanoff, P. *J. Phys. Chem. C* **2008**, *112*, 15356−15366.
(5) Bouwkamp-Wijnoltz, A. L.; Visscher, W.; van Veen, J. A. R.; Boellaard, E.; van der Kraan, A. M.; Tang, S. C. *J. Phys. Chem. B* **2002**, *106*, 12993−13001.
(6) Bae, I. T.; Tryk, D. A.; Scherson, D. A. *J. Phys. Chem. B* **1998**, *102*, 4114−4117.
(7) Schulenburg, H.; Stankov, S.; Schunemann, V.; Radnik, J.; Dorbandt, I.; Fiechter, S.; Bogdanoff, P.; Tributsch, H. *J. Phys. Chem. B* **2003**, *107*, 9034−9041.
(8) Bezerra, C. W. B.; Zhang, L.; Lee, K. C.; Liu, H. S.; Zhang, J. L.; Shi, Z.; Marques, A. L. B.; Marques, E. P.; Wu, S. H.; Zhang, J. J. *Electrochim. Acta* **2008**, *53*, 7703−7710.
(9) Liu, H. S.; Shi, Z.; Zhang, J. L.; Zhang, L.; Zhang, J. J. *J. Mater. Chem.* **2009**, *19*, 468−470.
(10) Choi, J.-Y.; Higgins, D.; Chen, Z. *J. Electrochem. Soc.* **2011**, *159*, B87−B90.
(11) Ye, S. Y.; Vijh, A. K. *Electrochem. Commun.* **2003**, *5*, 272−275.
(12) Lalande, G.; Cote, R.; Guay, D.; Dodelet, J. P.; Weng, L. T.; Bertrand, P. *Electrochim. Acta* **1997**, *42*, 1379−1388.
(13) Choi, J.-Y.; Hsu, R. S.; Chen, Z. *ECS Trans.* **2010**, *28*, 101−112.
(14) Choi, J.-Y.; Hsu, R. S.; Chen, Z. *J. Phys. Chem. C* **2010**, *114*, 8048−8053.
(15) Hsu, R. S.; Chen, Z. *ECS Trans.* **2010**, *28*, 39−46.
(16) Lefevre, M.; Dodelet, J. P.; Bertrand, P. *J. Phys. Chem. B* **2002**, *106*, 8705−8713.
(17) Wang, H.; Cote, R.; Faubert, G.; Guay, D.; Dodelet, J. P. *J. Phys. Chem. B* **1999**, *103*, 2042−2049.
(18) Cote, R.; Lalande, G.; Guay, D.; Dodelet, J. P.; Denes, G. *J. Electrochem. Soc.* **1998**, *145*, 2411−2418.
(19) Lefevre, M.; Dodelet, J. P.; Bertrand, P. *J. Phys. Chem. B* **2000**, *104*, 11238−11247.
(20) Jaouen, F.; Dodelet, J. P. *J. Phys. Chem. C* **2007**, *111*, 5963−5970.
(21) Chung, H. T.; Johnston, C. M.; Artyushkova, K.; Ferrandon, M.; Myers, D. J.; Zelenay, P. *Electrochem. Commun.* **2010**, *12*, 1792−1795.
(22) Lefevre, M.; Proietti, E.; Jaouen, F.; Dodelet, J. P. *Science* **2009**, *324*, 71−74.
(23) Zelenay, P.; Wu, G.; More, K. L.; Johnston, C. M. *Science* **2011**, *332*, 443−447.
(24) Lalande, G.; Faubert, G.; Cote, R.; Guay, D.; Dodelet, J. P.; Weng, L. T.; Bertrand, P. *J. Power Sources* **1996**, *61*, 227−237.
(25) Jaouen, F.; Herranz, J.; Lefevre, M.; Dodelet, J. P.; Kramm, U. I.; Herrmann, I.; Bogdanoff, P.; Maruyama, J.; Nagaoka, T.; Garsuch, A.; Dahn, J. R.; Olson, T.; Pylypenko, S.; Atanassov, P.; Ustinov, E. A. *ACS Appl. Mater. Interfaces* **2009**, *1*, 1623−1639.
(26) Titov, A.; Zapol, P.; Kral, P.; Liu, D. J.; Iddir, H.; Baishya, K.; Curtiss, L. A. *J. Phys. Chem. C* **2009**, *113*, 21629−21634.
(27) Franke, R.; Ohms, D.; Wiesener, K. *J. Electroanal. Chem.* **1989**, *260*, 63−73.
(28) Nallathambi, V.; Lee, J. W.; Kumaraguru, S. P.; Wu, G.; Popov, B. N. *J. Power Sources* **2008**, *183*, 34−42.
(29) Mitchell, R.; Moody, A. J.; Rich, P. R. *Biochemistry* **1995**, *34*, 7576−7585.
(30) Birry, L.; Zagal, J. H.; Dodelet, J. P. *Electrochem. Commun.* **2010**, *12*, 628−631.
(31) Gupta, S.; Fierro, C.; Yeager, E. *J. Electroanal. Chem.* **1991**, *306*, 239−250.
(32) Li, W. M.; Yu, A. P.; Higgins, D. C.; Llanos, B. G.; Chen, Z. W. *J. Am. Chem. Soc.* **2010**, *132*, 17056−17058.
(33) Thorum, M. S.; Hankett, J. M.; Gewirth, A. A. *J. Phys. Chem. Lett.* **2011**, *2*, 295−298.
(34) Schilt, A. A. *J. Am. Chem. Soc.* **1957**, *79*, 5421−5425.
(35) Schilt, A. A. *J. Am. Chem. Soc.* **1960**, *82*, 3000−3005.
(36) Milani, M.; Ouellet, Y.; Ouellet, H.; Guertin, M.; Boffi, A.; Antonini, G.; Bocedi, A.; Mattu, M.; Bolognesi, M.; Ascenzi, P. *Biochemistry* **2004**, *43*, 5213−5221.
(37) Li, J. F.; Lord, R. L.; Noll, B. C.; Baik, M. H.; Schulz, C. E.; Scheidt, W. R. *Angew. Chem., Int. Ed.* **2008**, *47*, 10144−10146.
(38) Leznoff, C. C.; Lever, A. P. B. *Phthalocyanines − Properties and Applications*; VCH Publishing: New York, 1996.
(39) Lu, X.; Hipps, K. W. *J. Phys. Chem. B* **1997**, *101*, 5391−5396.
(40) Beckstein, O.; Sansom, M. S. P. *Proc. Natl. Acad. Sci.* **2003**, *100*, 7063−7068.
(41) Eikerling, M.; Kornyshev, A. A.; Kucernak, A. R. *Phys. Today* **2006**, *59*, 38−44.
(42) Karyakin, A. A.; Karyakina, E. E.; Gorton, L. *Talanta* **1996**, *43*, 1597−1606.
(43) Gouerec, P.; Biloul, A.; Contamin, O.; Scarbeck, G.; Savy, M.; Riga, J.; Weng, L. T.; Bertrand, P. *J. Electroanal. Chem.* **1997**, *422*, 61−75.
(44) Wu, J.; Li, W.; Higgins, D.; Chen, Z. *J. Phys. Chem. C* **2011**, *115*, 18856−18862.